Journal of Hydrology 535 (2016) 54–60

Contents lists available at ScienceDirect

Journal of Hydrology

journal homepage: www.elsevier.com/locate/jhydrol

Mixed artificial grasslands with more roots improved mine soil infiltration capacity

Wu Gao-Lin [a,b,*,1], Yang Zheng [a,1], Cui Zeng [a], Liu Yu [a,b], Fang Nu-Fang [a,b], Shi Zhi-Hua [a,b,*]

[a] State Key Laboratory of Soil Erosion and Dryland Farming on the Loess Plateau, Institute of Soil and Water Conservation, Northwest A&F University, Yangling, Shaanxi 712100, China
[b] Institute of Soil and Water Conservation, Chinese Academy of Sciences and Ministry of Water Resources, Yangling, Shaanxi 712100, China

ARTICLE INFO

Article history:
Received 20 November 2015
Received in revised form 21 January 2016
Accepted 22 January 2016
Available online 2 February 2016
This manuscript was handled by Geoff Syme, Editor-in-Chief

Keywords:
Soil infiltration capacity
Artificial grassland
Soil infiltration capacity index (SICI)
Soil physical properties

SUMMARY

Soil water is one of the critical limiting factors in achieving sustainable revegetation. Soil infiltration capacity plays a vital role in determining the inputs from precipitation and enhancing water storage, which are important for the maintenance and survival of vegetation patches in arid and semi-arid areas. Our study investigated the effects of different artificial grasslands on soil physical properties and soil infiltration capacity. The artificial grasslands were *Medicago sativa*, *Astragalus adsurgens*, *Agropyron mongolicum*, *Lespedeza davurica*, *Bromus inermis*, *Hedysarum scoparium*, *A. mongolicum* + *Artemisia desertorum*, *A. adsurgens* + *A. desertorum* and *M. sativa* + *B. inermis*. The soil infiltration capacity index (SICI), which was based on the average infiltration rate of stage I (AIRSI) and the average infiltration rate of stage III (AIRS III), was higher (indicating that the infiltration capacity was greater) under the artificial grasslands than that of the bare soil. The SICI of the *A. adsurgens* + *A. desertorum* grassland had the highest value (1.48) and bare soil (−0.59) had the lowest value. It was evident that artificial grassland could improve soil infiltration capacity. We also used principal component analysis (PCA) to determine that the main factors that affected SICI were the soil water content at a depth of 20 cm (SWC20), the below-ground root biomasses at depths of 10 and 30 cm (BGB10, BGB30), the capillary porosity at a depth of 10 cm (CP10) and the non-capillary porosity at a depth of 20 cm (NCP20). Our study suggests that the use of Legume-poaceae mixtures and Legume-shrub mixtures to create grasslands provided an effective ecological restoration approach to improve soil infiltration properties due to their greater root biomasses. Furthermore, soil water content, below-ground root biomass, soil capillary porosity and soil non-capillary porosity were the main factors that affect the soil infiltration capacity.

1. Introduction

Mining and related activities have led to severe soil degradation and soil disturbance through mining operations that change soil properties and destroy soil structure (Shrestha and Lal, 2011; Yang et al., 2015). Surface mining operations should be followed by soil reclamation and/or the reestablishment of vegetative cover. Reclamation involves replacing top soil that was removed and homogenized followed by seeding. The most common post-mining land uses were for hay production and for providing pasture (Jeffrey et al., 2008). In abandoned quarries or surface mines, recolonization by plants was very difficult (Ballesteros et al., 2012) because of the destruction of the natural soil structure and of the seed bank, as well as the limitations of nutrients and water (Haritash et al., 2007). Soil water is one of the most critical limiting factors affecting plant growth and distribution patterns in semi-arid regions (Wang et al., 2008). Rainfall is the only source of soil water replenishment in desert ecosystems (Wang et al., 2007). Soil infiltration capacity plays a critical role in determining the precipitation inputs to the soil and in enhancing soil water storage, which is important for the maintenance and survival of vegetation patches in arid and semi-arid areas (David et al., 2015). Thus, soil infiltration capacity is an important soil hydrological parameter that can be used as an indicator of soil degradation and drought potential (Zhang et al., 2010). Therefore, it is very important to quantify the soil infiltration capacity.

Infiltration is the movement of water into the soil from the surface by downward or gravitational flow. The rate at which this occurs is known as the infiltration rate (Osuji et al., 2010). Several past studies have been conducted to determine infiltration rates in soil vegetated with different vegetation types in order to evaluate

* Corresponding authors at: State Key Laboratory of Soil Erosion and Dryland Farming on the Loess Plateau, Institute of Soil and Water Conservation, Northwest A&F University, Yangling, Shaanxi 712100, China.
E-mail addresses: gaolinwu@gmail.com (G.-L. Wu), shizhihua70@gmail.com (Z.-H. Shi).
[1] These authors contributed equally to this work.

http://dx.doi.org/10.1016/j.jhydrol.2016.01.059
0022-1694/

the soil infiltration capacity during the course of rainfall events. Soil infiltration capacity can determine, for example, the initial and steady infiltration rates, the mean infiltration rate, the water infiltration depth and accumulated infiltration (Zhao et al., 2013; Li et al., 2013; Bi et al., 2014 Liu et al., 2015). Christine et al. (2014) used a hood infiltrometer for in situ infiltration measurements and evaluated the infiltration capacity of grassland indirectly through different parts of the pore spectrum. However, the use of only one or two parameters could not comprehensively evaluate the soil infiltration capacity. In view of these issues, a better understanding of the infiltration capacity under different grasslands during vegetation restoration is considered important to the sustainable eco-environmental construction on reclaimed mine soils.

Many studies have found that the infiltration capacity of soil was mainly controlled by both vegetation characteristics and soil physical properties (Wang et al., 2003; Christine et al., 2014; Leung et al., 2015). Li et al. (2013) reported that the soil permeability had significant positive linear correlations with the total porosity, non-capillary porosity, initial water content, and water holding capacity of the soil, and a significant negative linear correlation with soil bulk density. Scanlan and Hinz (2010) found that plant roots could clog soil pores and decrease the soil infiltration rate. However, previous studies on the relationship between soil infiltration capacity and structural properties were mostly based on laboratory experiments using disturbed and sieved-soil. Quantitative information about the soil infiltration capacity as affected by the structural properties under field conditions is scarce.

In view of the close relationship between soil physical properties and soil infiltration capacity, we assumed that (1) artificial grassland with a greater root biomass could more effectively improve soil infiltration capacity by improving soil infiltration rates; and (2) we studied soil infiltration rates and soil physical properties to find the main factors that affected soil infiltration. The results should provide new insights into the effects of vegetation restoration on infiltration and further provide a baseline reference for rational vegetation restoration and soil–water conservation in the mining areas.

2. Materials and methods

2.1. Study sites

The present study was conducted in the dump area of the Yongli coal mine, Inner Mongolian Autonomous Region, which is located on the northern Loess Plateau (110°16′30″E, 39°41′52″N, H: 1026–1304 m) in China. The area is characterized by a semiarid climate, with a mean annual temperature of 7.2 °C and a mean annual precipitation of 404.1 mm, which mostly occurs from July to September and accounts for about 80% of the annual rainfall. The annual evaporation is 2082.2 mm. The annual cloud-free solar radiation is about 3119.3 h. The climate is cold and dry in the winter and spring, and hot and rainy in the summer. The main soil type is a sandy soil (Calcaric Cambisols, FAO) and the thickness of the soil layer is about 50 cm. The main plant species in the region are *Artemisia sacrorum*, *Stipa capillata*, *Artemisia desterorum*, and *Lespedeza bicolor*.

2.2. Experiment design

Nine-types of artificial grasslands were established on the reclaimed land: *Medicago sativa*, *Astragalus adsurgens*, *Agropyron mongolicum, Lespedeza davurica, Bromus inermis, Hedysarum scoparium, A. mongolicum + Artemisia desertorum*, *A. adsurgens + A. desertorum* and *M. sativa + B. inermis*. *M. sativa* and *B. inermis*. These are the most common species used in vegetation restoration and can improve soil properties relatively quickly. *A. adsurgens*, *A. mongolicum*, *L. davurica* and *H. scoparium* are also dominant native species of this region and are adapted to survive in arid environments. *A. desertorum* is a pioneer species of community succession, which can be used as an indicator of the soil status. Six replicate plots (3 m × 5 m) were established in each grassland type. Seeding was carried out with a row spacing of 50 cm and at a sowing rate 0.07 kg/m^2. Due to the barrenness of the soil, the sowing rate was a little higher than usual in order to guarantee an adequate emergence rate, which would also increase the population density that could rapidly cover and protect the soil surface. Revegetation of the various grasses used the same planting density and the plants were irrigated to ensure grass survival during the beginning of the restoration period. Later on, grass growth entirely depended on rainfall, without fertilization or human intervention. This ensured that the conditions in all of the plots were similar during the experiment but also that any differences were solely due to the grassland type. Hence, it could be assumed that any differences in soil infiltration could be attributed to the type of artificial grassland.

From the beginning of the growing season, we randomly selected three parallel 1 m × 1 m quadrats in each of the plots at two-month intervals. Aboveground biomass was harvested from each quadrat by cutting the plant stems at the soil level, and was then sealed in an envelope. Each envelope was weighed while the plant material was fresh and then re-weighed after drying at 65 °C for 48 h. To measure the below-ground root biomass, a 9-cm diameter root augur was used to remove three soil samples from each soil depth of 0–10, 10–20, and 20–30 cm. The three samples collected from the same layer were then mixed to create a single composite sample. A 2-mm sieve was used to separate most of the plant roots from the soil. No attempt was made to distinguish between living and dead roots. The separated roots were oven-dried at 75 °C for 48 h and then weighed.

2.3. Soil properties analysis

The thickness of mine soil is about 50 cm and plant roots are mainly distributed in the 0–30 cm soil layer (Leung et al., 2015) and the depth of rainfall infiltration is about 30 cm (Liu et al., 2015). Therefore, we investigated soil properties in the 0–30 cm layer. The soil bulk density of each layer (0–10, 10–20, 20–30 cm) was measured for soil samples using a stainless steel cutting ring, 5 cm in diameter and 5 cm in depth (3 replicates) to collect a known volume of undisturbed soil. The dry mass was measured after oven-drying at 105 °C and the bulk density was calculated. Soil water content was measured gravimetrically and expressed as a ratio of soil water to dry soil mass. Total soil porosity (TP) was calculated using Eq. (1) based on the measured bulk density and assuming a soil particle density of 2.65 g cm^{-3}. Soil capillary porosity (CP) was subsequently calculated using Eq. (2) and the bulk density and soil capillary water capacity data (Jiao et al., 2011). Soil non-capillary porosity (NCP) was calculated using Eq. (3) (Huang, 2003).

$$\mathrm{TP} = \left(1 - \frac{\mathrm{BD}}{ds}\right) \times 100 \quad (1)$$

where TP is the total soil porosity (%); BD is the soil bulk density (g cm^{-3}); and *ds* is the soil particle density (g cm^{-3})

$$\mathrm{CP} = W_c \times \frac{\mathrm{BD}}{V} \times 100 \quad (2)$$

$$\mathrm{NCP} = \mathrm{TP} - \mathrm{CP} \quad (3)$$

where CP is the soil capillary porosity (%); NCP is the soil non-capillary porosity (%); W_c is the soil capillary water content (%); and V is the volume of the soil core (cm^3).

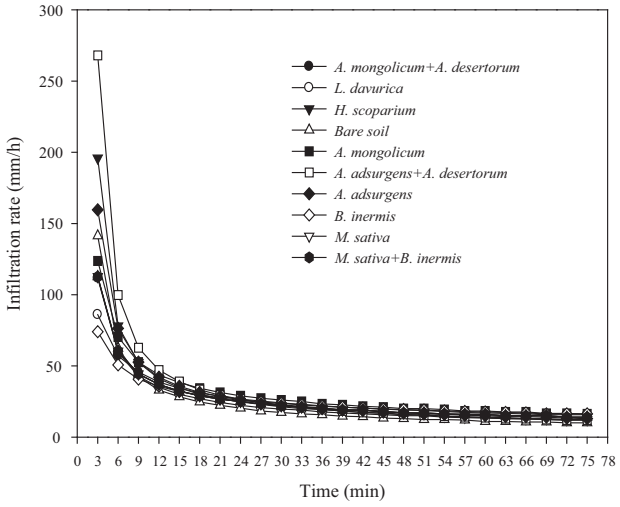

Fig. 1. Soil infiltration rates under different artificial grasslands.

2.4. Soil infiltration rate measurement

The soil infiltration rates under the different artificial grasslands were determined using a soil infiltration capacity automatic measurement system (Mao et al., 2011; Lei et al., 2013). This system comprises a camera, a computer, a peristaltic pump and a tripod. As the peristaltic pump supplies water to the soil surface at a constant known rate, the camera automatically captures images of the expanding wet area every 3 min under the control of the computer. We used a numerical algorithm to calculate the soil infiltration capacity based on the rate at which the wet front advanced (Lei et al., 2007, 2010, 2013). The numerical algorithm model calculated the infiltration rate at different times (Lei et al., 2010, 2013). The soil infiltration rate is given by

$$i_n = \frac{q - \sum_{j=1}^{n-1} i_j \Delta A_{n-j+1}}{\Delta A_n} \quad (n = 1, 2, 3 \ldots) \tag{4}$$

where q is water flow rate, L/h (in this study, the water flow rate was set at 3 L/h based on the study of Sun et al. (2013); I_n is the soil infiltration rate at time n, t_n, mm/h; and ΔA_n is the increase in the wet area for a given time period ($t_n - t_{n-1}$), mm^2.

According to the process of soil infiltration (Fig. 1), we took the mean infiltration rate of the first 3 min as the initial infiltration rate (IIR), and then took the average infiltration rate of 0–15 min as the average infiltration rate of stage I (AIRSI). Likewise, the average infiltration rate of stage II (AIRS II) was for the period 15–45 min and the average infiltration rate of stage III (AIRS III) was for the period 45–75 min. The average infiltration rate of the final 3 min was taken as the steady infiltration rate (SIR). The average infiltration rate of the 0–75 min period was taken as the overall average infiltration rate (AIR).

Table 2
Principal component analysis of soil infiltration rate of different artificial grasslands.

Principal component	PC-1	PC-2
Eigenvalue	3.388	2.598
Variance	56.461	43.302
Cumulative	56.461	99.763
Eigenvectors		
The average infiltration rate (AIR)	0.614	0.789
The average infiltration rate in stage I (AIRSI)	−0.035	**0.999**
The average infiltration rate in stage II (AIRS II)	0.985	0.161
The average infiltration rate in stage III (AIRS III)	**0.991**	−0.128
The initial infiltration rate (IIR)	−0.312	0.948
The steady infiltration rate (SIR)	0.979	−0.190

Note: Bold-faced parameters are considered as the critical ones and were included in the soil infiltration capacity index calculation.

Table 3
Correlation matrix among the different infiltration rates determined.

Parameters	AIR	AIRSI	AIRS II	AIRS III	IIR	SIR
AIR	1					
AIRSI	0.727**	1				
AIRS II	0.884**	0.325	1			
AIRS III	0.785**	0.148	0.978**	1		
IIR	0.348*	0.889**	−0.129	−0.290	1	
SIR	0.759**	0.111	0.967**	0.998**	−0.320	1

Note: AIR: The average infiltration rate; AIRSI, AIRS II and AIRS III: The average infiltration rate in stage I, II and III; IIR: The initial infiltration rate; SIR: The steady infiltration rate.
* Correlation is significant at the $p < 0.05$ level (2-tailed).
** Correlation is significant at the $p < 0.01$ level (2-tailed).

2.5. Soil infiltration capacity index

As previously mentioned, soil infiltration comprises a variety of processes that cannot be assessed by one parameter alone, but requires a variety of parameters. However, some parameters are correlated significantly with each other and usually reflect the same information; thus it is necessary to identify and eliminate these redundant parameters. An integrated SICI was employed in the present study. The method involved three main steps: (1) selecting the appropriate parameters; (2) transforming and weighting the parameters; and (3) combining the parameter scores into an index. Parameters that differed significantly were chosen for the SICI calculation. The choice of appropriate parameters and their weighting were determined by principal component analysis

Table 1
Soil infiltration rates (mean ± SD) of different artificial grasslands.

Functional group	Artificial grassland types	AIR	AIRSI	AIRS II	AIRS III	IIR	SIR
Grass-shrub	*A. mongolicum + A. desertorum*	26.93 ± 4.60	52.33 ± 7.60a	24.17 ± 4.26	17 ± 3.44	86 ± 12.34a	15.67 ± 3.28
Legumes-shrub	*A. adsurgens + A. desertorum*	35.25 ± 4.48	103.27 ± 19.02b	22.87 ± 3.06	13.63 ± 2.22	268 ± 67.00b	12 ± 2.08
Legumes-grass	*M. sativa + B. inermis*	26.85 ± 2.51	49.93 ± 1.53a	24.33 ± 2.94	17.83 ± 2.74	82 ± 4.51a	16.33 ± 2.60
Shrub	*H. scoparium*	30.32 ± 1.63	80.4 ± 8.42ab	21.77 ± 4.50	13.83 ± 3.53	196 ± 56.59ab	12.33 ± 3.18
Grass	*B. inermis*	25.81 ± 1.98	46.6 ± 1.22a	23.67 ± 2.30	17.57 ± 2.14	74 ± 3.06a	16.33 ± 2.03
	A. mongolicum	30.85 ± 6.00	65.73 ± 16.13ab	26.17 ± 4.85	18.1 ± 3.42	123.67 ± 39.03ab	16.33 ± 2.96
Legumes	*L. davurica*	24.47 ± 4.51	55.8 ± 6.11ab	19.97 ± 4.86	13.3 ± 3.88	111.67 ± 11.35ab	12 ± 3.61
	A. adsurgens	29.85 ± 5.87	73.27 ± 5.72ab	23.1 ± 6.67	14.9 ± 5.14	159.67 ± 7.75ab	13 ± 4.73
	M. sativa	26.6 ± 1.88	57.33 ± 7.10ab	22.3 ± 3.33	15.53 ± 3.60	112.67 ± 30.19ab	14 ± 3.61
Bare soil	Bare soil	23.91 ± 7.13	61.47 ± 11.40ab	17.73 ± 7.22	11.3 ± 5.08	141.33 ± 15.76ab	10 ± 4.58

Note: AIR: The average infiltration rate (0–75 min); AIRSI, AIRS II and AIRS III: The average infiltration rates during stage I (0–15 min), II (15–45 min) and III (45–75 min); IIR: The initial infiltration rate (0–3 min); SIR: The steady infiltration rate (72–75 min).
Values followed by a different letter were significantly different at the $p < 0.05$ level.

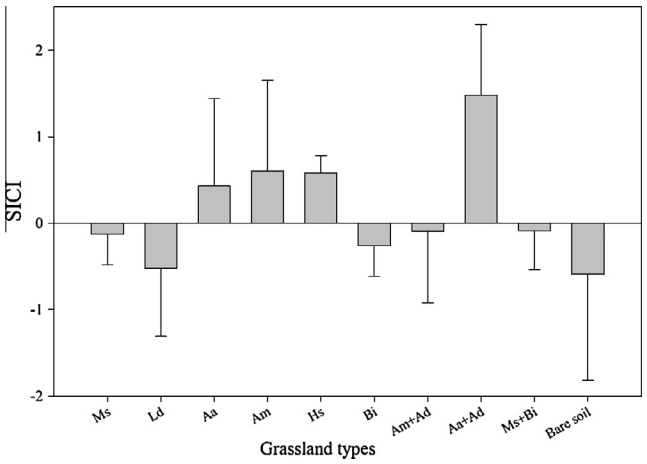

Fig. 2. Soil infiltration capacity index (SICI) of different artificial grasslands. *M. s.* (*Medicago sativa*), *L. d.* (*Lespedeza davurica*), *A. a.* (*Astragalus adsurgens*), *A. m.* (*Agropyron mongolicum*), *H. s.* (*Hedysarum scoparium*), *B. i.* (*Bromus inermis*), *A. m.* + *A. d.* (*Agropyron mongolicum* + *Artemisia desertorum*) *A. a.* + *A. d.* (*Astragalus adsurgens* + *Artemisia desertorum*) and *M. s.* + *B. i.* (*Medicago sativa* + *Bromus inermis*).

(PCA). From each principal component (PC), the parameters with higher loading values were chosen. From any given PC, we selected parameters that did not correlate with others (as determined by Pearson correlation analysis) within that PC when more than one parameter had a high loading value. If the parameters exhibited a high degree of correlation, the one with the higher loading value was finally chosen for the determination of the SICI.

$$\mathrm{SICI} = \sum_{i=1}^{n} WiYi \tag{5}$$

In Eq. (5), W is the weighting factor of the parameter selected through the PCA; and Y is the score of the proposed parameter after conversion.

2.6. Statistical analysis

All data were expressed as mean ± standard error of the mean. Statistical analyses were conducted using SPSS software (ver.16.0). The differences in the values of the soil infiltration rates among the different grassland types were compared by using the one-way analysis of variance (ANOVA) procedure. Significant differences were evaluated at the 0.05 level.

3. Results

3.1. Soil infiltration rates

The artificial grasslands had higher values of AIR, AIRS II, AIRS III and SIR than the bare soil had (Fig. 1; Table 1). Compared with bare soil, these values were improved by 2.3–47.4%, 12.6–47.6%, 17.7–60.2% and 20–63.3%, respectively. The AIR of *A. Adsurgens* + *A. desertorum* grassland (35.25 ± 4.48 mm/h) had the highest value. Both the AIRS II, and AIRS III of *A. mongolicum* grassland (26.17 ± 4.85 mm/h, 18.1 ± 3.42 mm/h) had the highest values. The *A. mongolicum*, *B. inermis* and *M. sativa* + *B. inermis* grasslands had higher SIR values. The IIR and AIRSI of *A. Adsurgens* + *A. desertorum* grassland had the highest values (268 ± 67.00 mm/h, 103.27 ± 19.02 mm/h), the lowest value occurred in the *B. inermis* grassland (74 ± 3.06 mm/h, 46.6 ± 1.22 mm/h). The AIRSI ($F = 2.755$, $P = 0.023$) and IIR ($F = 3.285$, $P = 0.01$) of artificial grasslands exhibited differences, while AIR, AIRS II, AIRS III and SIR of grasslands were not significantly different.

3.2. Soil infiltration capacity index

As shown in Table 2, the eigenvalues of the first two PCs were above 1. The more highly weighted parameters in PC-1 were SIRS II, SIRS III and SSIR. The SIRS III had the highest loading value but there was also a strong correlation between it and both SIRS II and SSIR ($r > 0.95$; Table 3). Thus, SIRS II and SSIR were eliminated from the SICI. In PC-2, the highly loaded parameters included ASIR, SIRSI and ISIR. The SIRSI had the highest loading value but was strongly correlated with both ASIR ($r = 0.73$; Table 3) and ISIR ($r = 0.89$; Table 3). Accordingly, SIRSI was chosen to be included in the calculation of the SICI. In summary, the most critical parameters as determined from the PCA for the SICI determination were SIRS III and SIRSI (Table 2). The scores of each PC were calculated from Eq. (6):

$$Y_{\mathrm{PC\text{-}1}} = -0.02Y_{\mathrm{SIRS\ I}} + 0.54_{\mathrm{SIRS\ III}} \tag{6}$$

Table 4
Principal component analysis of soil properties of different artificial grasslands.

Principal component	PC-1	PC-2	PC-3	PC-4
Eigenvalue	10.128	3.558	1.616	1.211
Variance	56.269	19.768	8.978	6.726
Cumulative	56.269	76.037	85.015	91.742
Eigenvectors				
Soil water content at depth of 10 cm (SWC10)	−0.934	−0.180	−0.056	0.100
Soil water content at depth of 20 cm (SWC20)	**−0.947**	−0.106	0.004	−0.017
Soil water content at depth of 30 cm (SWC30)	−0.864	0.022	0.072	−0.359
Bulk density at depth of 10 cm (BD10)	−0.838	−0.071	−0.386	0.310
Bulk density at depth of 20 cm (BD20)	−0.861	−0.160	0.367	0.240
Bulk density at depth of 30 cm (BD30)	−0.926	−0.277	0.121	−0.056
Below-ground biomass at depth of 10 cm (BGB10)	0.631	−0.035	**0.672**	0.163
Below-ground biomass at depth of 20 cm (BGB20)	0.692	−0.384	−0.114	0.472
Below-ground biomass at depth of 30 cm (BGB30)	0.639	0.168	0.127	**0.637**
Total porosity at depth of 10 cm (TP10)	0.836	0.071	0.389	−0.312
Total porosity at depth of 20 cm (TP20)	0.861	0.160	−0.365	−0.241
Total porosity at depth of 30 cm (TP30)	0.926	0.277	−0.121	0.056
Capillary porosity at depth of 10 cm (CP10)	0.610	**−0.706**	−0.219	−0.135
Capillary porosity at depth of 20 cm (CP20)	0.772	−0.549	−0.075	−0.146
Capillary porosity at depth of 30 cm (CP30)	0.842	−0.425	0.085	−0.093
Non-capillary porosity at depth of 10 cm (NCP10)	−0.012	0.812	0.534	−0.095
Non-capillary porosity at depth of 20 cm (NCP20)	0.072	**0.88**	−0.346	−0.107
Non-capillary porosity at depth of 30 cm (NCP30)	0.216	0.842	−0.252	0.179

Note: Bold-faced parameters are considered as the critical ones that affect soil infiltration capacity.

Table 5
Correlation matrix among the difference infiltration rates determined.

	BD10	BD20	BD30	BGB10	BGB20	BGB30	SWC10	SWC20	SWC30	TP10	CP10	NCP10	TP20	CP20	NCP20	TP30	CP30	NCP30
BD10	1																	
BD20	0.76**	1																
BD30	0.80**	0.87**	1															
BGB10	−0.56**	−0.30	−0.48**	1														
BGB20	−0.23	−0.30	−0.31	0.45**	1													
BGB30	−0.19	−0.17	−0.31	0.49**	0.81**	1												
SWC10	0.69**	0.70**	0.80**	−0.58**	−0.56**	−0.55**	1											
SWC20	0.70**	0.74**	0.84**	−0.58**	−0.63**	−0.55**	0.94**	1										
SWC30	0.52**	0.60**	0.75**	−0.55**	−0.67**	−0.58**	0.77**	0.82**	1									
TP10	−0.99**	−0.76**	−0.80**	0.56**	0.23	0.18	−0.69**	−0.69**	−0.52**	1								
CP10	−0.57**	−0.60**	−0.50**	0.40*	0.50**	0.16	−0.46**	−0.48**	−0.48**	0.57**	1							
NCP10	−0.31	−0.04	−0.20	0.08	−0.35*	−0.03	−0.13	−0.12	0.05	0.317	−0.60**	1						
TP20	−0.76**	−1.00**	−0.87**	0.29	0.29	0.17	−0.70**	−0.74**	−0.60**	0.76**	0.60**	0.04	1					
CP20	−0.58**	−0.67**	−0.67**	0.34	0.33	0.05	−0.55**	−0.63**	−0.58**	0.58**	0.71**	−0.23	0.67**	1				
NCP20	−0.31	−0.53**	−0.40*	−0.08	−0.07	0.11	−0.29	−0.23	−0.10	0.31	−0.08	0.41*	0.53**	−0.25	1			
TP30	−0.80**	−0.87**	−1.00**	0.48**	0.317	0.31	−0.80**	−0.84**	−0.75**	0.80**	0.50**	0.20	0.87**	0.67**	0.40*	1		
CP30	−0.53**	−0.49**	−0.54**	0.36*	0.36*	0.23	−0.63**	−0.67**	−0.59**	0.53**	0.39*	0.11	0.49**	0.75**	−0.09	0.54**	1	
2bNCP30	−0.48**	−0.58**	−0.69**	0.24	0.04	0.17	−0.38*	−0.40*	−0.35*	0.48**	0.24	0.25	0.58**	0.22	0.69**	0.69**	−0.24	1

Note: SWC10, 20, 30: Soil water content at depths of 10, 20 and 30 cm; BD10, 20, 30: Bulk density at depths of 10, 20 and 30 cm; BGB10, 20, 30: Below-ground biomass at depths of 10, 20 and 30 cm; TP10, 20, 30: Total porosity at depths of 10, 20 and 30 cm; CP10, 20, 30: Capillary porosity at depths of 10, 20 and 30 cm; NCP10, 20, 30: Non-capillary porosity at depths of 10, 20 and 30 cm.
* Correlation is significant at the $p < 0.05$ level (2-tailed).
** Correlation is significant at the $p < 0.01$ level (2-tailed).

$$Y_{PC\text{-}2} = 0.62Y_{SIRS\ I} - 0.08_{SIRS\ III} \quad (7)$$

The final polynomial for the SICI was calculated from Eq. (8):

$$SICI = 0.2734Y_{SIRS\ III} + 0.2552Y_{SIRS\ I} \quad (8)$$

where Y is the score of the critical parameters.

As shown in Fig. 2, the SICI was different for the artificial grassland types. The *A. Adsurgens + A. desertorum* grassland had the highest value (1.48), followed by *A. mongolicum* (0.60), *H. scoparium* (0.58) and *A. adsurgens* (0.43), while the lowest value was determined for the bare soil (−0.59). There were no significant differences among the SICI of the artificial grasslands.

3.3. Soil properties affecting infiltration capacity

As shown in Table 4, the eigenvalues of the first four PCs were great than 1. The highly weighted parameters in PC-1 were SWC10, SWC20, BD30 and TP30. The SWC20 had the highest loading value and was strongly correlated with SWC10, BD30 and TP30 (Table 5). Thus, SWC10, BD30 and TP30 were eliminated, while SWC20 was retained as a parameter that affected the soil infiltration capacity. In PC-2, the highly loaded parameters included NCP10, NCP20, NCP30 and CP10. The NCP20 had the highest loading value and was strongly correlated with NCP10 ($r = 0.41$; Table 5) and NCP30 ($r = 0.69$; Table 5). No significant correlation was found between CP10 and NCP20 ($r = -0.08$); therefore, both NCP20 and CP10 were selected. Likewise, BGB10 and BGB30 were chosen due to their higher loading values in PC-3 and PC-4. In summary, the most critical parameters, as determined from the PCA, that would affect soil infiltration capacity were SWC20, NCP20, CP10, BGB10 and BGB30 (Table 4).

As shown in Fig. 3, the SWC20 under the artificial grasslands were significant lower than that under the bare soil ($F = 5.806$, $P < 0.01$). The SWC20 under bare soil (18.17%) was the highest, followed by *L. davurica* (12.27%), while *H. scoparium* grassland (9.78%) had the lowest SWC20. There were no significant differences among nine types of artificial grasslands.

The BGB10 of *B. inermis* grasslands (2123.5 ± 553.50 g/m^2) was the largest followed by *H. scoparium* grassland (1744.7 ± 57.74 g/m^2) and *A. mongolicum* grassland (1607.6 ± 342.05 g/m^2), while the smallest BGB10 was found under *L. davurica* grassland (297.65 ± 49.54 g/m^2). There were significant differences among BGB10 under the artificial grasslands ($F = 2.546$, $P = 0.022$). In contrast, the BGB30 under the artificial grasslands did not differ significantly. The BGB30 under *M. sativa* grassland (104.41 ± 40.80 g/m^2) was the largest and was larger than the smallest BGB30, which was under *L. davurica* grassland (21.76 ± 11.57 g/m^2), by about 5 times.

The CP10 under all of the artificial grasslands was higher than that of the bare soil (30.84%). The CP10 under *H. scoparium* grassland (43.85%) was the highest, followed by *M. sativa + B. inermis* (40.10%) and *A. Mongolicum + A. desertorum* grassland (37.89%). The CP10 under the *B. inermis* grassland (31.31%) was the lowest, and was only 1.5% higher than that of the bare soil. There were significant differences among the CP10 under the artificial grasslands ($F = 3.823$, $P = 0.004$). For NCP20, that under the *H. scoparium* grassland (0.44%) was the lowest and those of the other artificial grasslands were higher than that of the bare soil (4.9%); the NCP20 under the *L. davurica* grassland (11.4%) was the highest. The NCP20 under the artificial grasslands were significantly different ($F = 14.969$, $P < 0.01$).

4. Discussion

Many studies have analyzed soil infiltration capacity using different parameters. However, the large number of studied sites and the high variability of the investigated physical, chemical and bio-

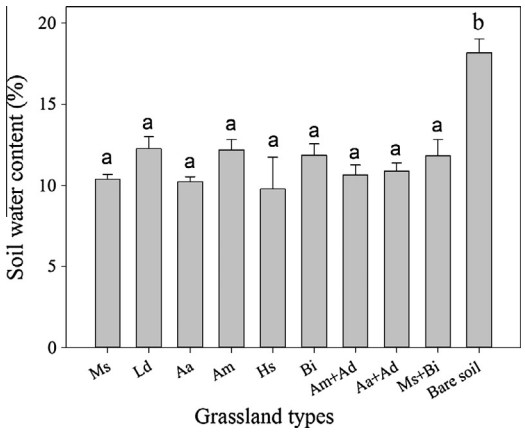

Fig. 3. Soil water content at a depth of 20 cm (mean ± SD) for different artificial grasslands. Values with a different letter are significantly different at the $p < 0.05$ level. *M. s.* (*Medicago sativa*), *L. d.* (*Lespedeza davurica*), *A. a.* (*Astragalus adsurgens*), *A. m.* (*Agropyron mongolicum*), *H. s.* (*Hedysarum scoparium*), *B. i.* (*Bromus inermis*), *A. m. + A. d.* (*Agropyron mongolicum + Artemisia desertorum*) *A. a. + A. d.* (*Astragalus adsurgens + Artemisia desertorum*) and *M. s. + B. i.* (*Medicago sativa + Bromus inermis*).

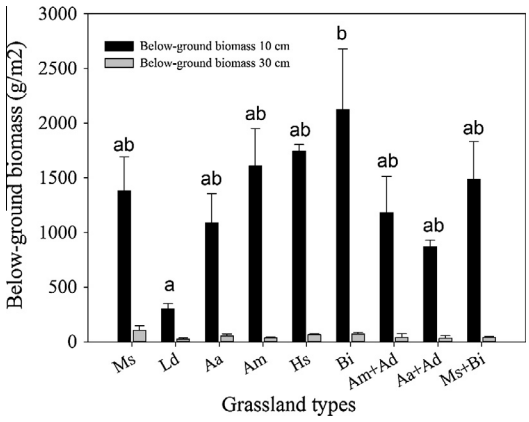

Fig. 4. Below-ground biomass at depths of 10 and 30 cm (mean ± SD) for different artificial grasslands. Columns with a different letter are significantly different at the $p < 0.05$ level. *M. s.* (*Medicago sativa*), *L. d.* (*Lespedeza davurica*), *A. a.* (*Astragalus adsurgens*), *A. m.* (*Agropyron mongolicum*), *H. s.* (*Hedysarum scoparium*), *B. i.* (*Bromus inermis*), *A. m. + A. d.* (*Agropyron mongolicum + Artemisia desertorum*) *A. a. + A. d.* (*Astragalus adsurgens + Artemisia desertorum*) and *M. s. + B. i.* (*Medicago sativa + Bromus inermis*).

logical indicators made it difficult to clearly interpret the results. We used a different approach that derived an index, SICI, as well as using a multivariate analysis to determine the parameters to be used in the SICI (PCA). Two parameters were finally selected for use in the SICI calculation that we considered the most important indicators of soil infiltration capacity (SIRS III and SIRSI). Using PCA, we also found that the main factors that affected soil infiltration capacity were SWC20, BGB10, BGB30, CP10 and NCP20. Previous studies also found that various soil properties and vegetation parameters had great affects on infiltration, e.g., soil water, bulk density, porosity and roots (Wang et al., 2007; Bormann and Klaassen, 2008; Li et al., 2013; Christine et al., 2014). These indicators were consistent with our results, which proved that our approach was reasonable.

In our study, the SICI of *A. adsurgens + A. desertorum* grassland was higher than that of *A. adsurgens* grassland, while the infiltration capacity was lower under the *A. mongolicum + A. desertorum* grassland than under the *A. mongolicum* grassland (Fig. 2). Sowing the seed mixtures of shrub and herbaceous species suppressed the growth of the shrubs. The reduced ratio of shrub to herbaceous species and the greater seeding density could affect the stability of the plant community (Feng et al., 2015). The BGB10 under *A. mongolicum + A. desertorum* and *A. adsurgens + A. desertorum* grasslands were smaller than those under *A. mongolicum* and *A. adsurgens* grasslands (Fig. 4). However, root induced pores differed with the plant species (Meek et al., 1989). The infiltration capacity was strongly affected by the presence of certain plant functional groups (Wu et al., 2014), such as grasses (*A. mongolicum*) and legumes (*M. sativa*). It has been reported that the infiltration capacity is increased by legumes and decreased by grasses (Archer et al., 2002; Christine et al., 2014). However, our results showed the opposite tendency. This might be because, in our study, we could not consider the effects of the shrub (*A. desertorum*) on the spatial patterns of infiltration (David et al., 2015). In addition, soil under a shrub canopy had a greater macroporosity and higher infiltration rate than soil without a shrub canopy. With the growth of the shrub, soil macroporosity decreased and soil infiltration capacity declined at the same time (Hu et al., 2015). Another reason was that the influences of the plant functional groups on soil infiltration changed during the growing season (Christine et al., 2014).

The soil infiltration capacity was higher under the *M. sativa* and *A. adsurgens* grasslands than under the *B. inermis* grassland. The BGB10 was much smaller under the *M. sativa* and *A. adsurgens* grasslands than under the *B. inermis* grassland. The *B. inermis* (grass species) grassland had many fibrous and rhizomatous roots, which tended to reduce infiltration by clogging the soil pore space and blocking water flow (Archer et al., 2002). The BGB30 was larger under the *M. sativa* and *A. adsurgens* grasslands than under the *B. inermis* grassland. Decaying tap-roots due to root proliferation under the two former grasslands formed stable macropores, which also increased soil organic matter content and encouraged the activity of soil fauna, such as earthworms, that formed even larger and longer macropores (Obi, 1999). That the NCP20 was higher under the *M. sativa* and *A. adsurgens* grasslands than under *B. inermis* grassland was also proof of this mechanism (Fig. 5). Soil infiltration capacity had a positive correlation with NCP (Li et al., 2013). All of these factors would increase infiltration capacity to different extents. The relationship of initial soil water content (10 cm) to the infiltration capacity was not clear (Archer et al., 2002; Li et al., 2013). The SWC10 was susceptible to changes by the external environment, such as rainfall, temperature and vegetation type. In arid regions, the topsoil layer was dry, while the soil

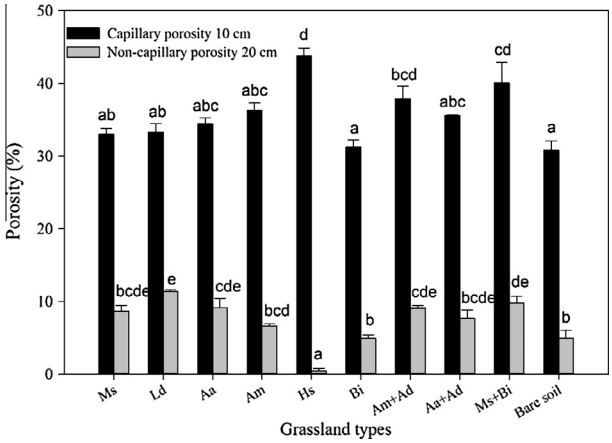

Fig. 5. Soil capillary porosity at depth of 10 cm and Non-capillary porosity at depth of 20 cm (mean ± SD) for different artificial grasslands. Values with a different letter are significantly different at the $p < 0.05$ level. *M. s.* (*Medicago sativa*), *L. d.* (*Lespedeza davurica*), *A. a.* (*Astragalus adsurgens*), *A. m.* (*Agropyron mongolicum*), *H. s.* (*Hedysarum scoparium*), *B. i.* (*Bromus inermis*), *A. m. + A. d.* (*Agropyron mongolicum + Artemisia desertorum*) *A. a. + A. d.* (*Astragalus adsurgens + Artemisia desertorum*) and *M. s. + B. i.* (*Medicago sativa + Bromus inermis*).

water content of the soil layer below it (SWC20) was higher and, with the increase in the hydraulic gradient, the upward movement of water led to the soil becoming generally dryer and increased the potential for infiltration (Alaoui, 2015). Therefore, when the SWC20 was lower, the infiltration capacity was higher.

5. Conclusions

Different artificial grasslands with different root biomasses significantly affected the soil physical properties and soil infiltration capacity of a mine soil. Compared with the bare soil, artificial grasslands with a larger root biomass more effectively improved the infiltration capacity of the mine soil. The larger root biomasses of *M. sativa + B. inermis* and *A. adsurgens + A. desertorum* grasslands led to higher soil infiltration capacities than those under *M. sativa, B. inermis* and *A. adsurgens* grasslands. Grasslands with legumes-poaceae mixtures and legumes-shrub mixtures had the higher soil infiltration capacities. The PCA method determined that the SIRS III and SIRSI were the two main evaluation indexes for the soil infiltration capacity. In addition, our results showed that soil water content, below-ground root biomass, soil capillary porosity and soil non-capillary porosity were the main factors that affected the soil infiltration capacity in this study. The soil infiltration capacity index proved itself to be a useful tool in evaluating the effect of artificial grasslands on soil infiltration capacity. Our approach of using soil infiltration capacity index in conjunction with PCA could be applied to other areas of research.

Acknowledgements

This research was funded by Projects of Natural Science Foundation of China (NSFC41525003, 41371282, 41390463), the Action Plan for West Development Project of CAS (KZCX2-XB3-13), the "Light of West China" Program of CAS (XAB2015A04) and Project of Natural Science Foundation of Shaanxi Province (2014KJXX-15).

References

Alaoui, A., 2015. Modelling susceptibility of grassland soil to macropore flow. J. Hydrol. 525, 536–546.
Archer, N.A.L., Quinton, J.N., Hess, T.M., 2002. Below-ground relationships of soil texture, roots and hydraulic conductivity in two-phase mosaic vegetation in South-east Spain. J. Arid Environ. 52, 535–553.
Ballesteros, M., Cañadas, E.M., Foronda, A., Fernández-Ondoño, E., Peñas, J., Lorite, J., 2012. Vegetation recovery of gypsum quarries: short-term sowing response to different soil treatments. Appl. Vege. Sci. 15, 187–197.
Bi, Y.L., Zou, H., Zhu, C.W., 2014. Dynamic monitoring of soil bulk density and infiltration rate during coal mining in sandy land with different vegetation. Int. J. Coal Sci. Technol. 1 (2), 198–206.
Bormann, H., Klaassen, K., 2008. Seasonal and land use dependent variability of soil hydraulic and soil hydrological properties of two Northern German soils. Geoderma 145, 295–302.
Christine, F., Christiane, R., Britta, J., Nico, E., Jussi, B., Sabine, A., Stefan, S., Wolfgang, W.W., Jens, S., Anke, H., 2014. How do earthworms, soil texture and plant composition affect infiltration along an experimental plant diversity gradient in grassland. PLoS ONE 9 (6), e98987.
David, J.E., Wang, L.X., Marta, R.C., 2015. Shrub encroachment alters the spatial patterns of infiltration. Ecohydrology 8, 83–93.
Feng, J., Zhang, C., Zhao, T., Zhang, Q., 2015. Rapid revegetation by sowing seed mixtures of shrub and herbaceous species. Solid Earth 6, 573–581.
Haritash, A.K., Baskar, R., Sharma, N., Paliwal, S., 2007. Impact of slate quarrying on soil properties in semi-arid Mahendragarh in India. Environ. Geol. 51, 1439–1445.
Hu, X., Li, Z.C., Li, X.Y., Liu, Y., 2015. Influence of shrub encroachment on CT-measured soil macropore characteristics in the Inner Mongolia grassland of northern China. Soil Till. Res. 150, 1–9.
Huang, C.Y., 2003. Soil Science. China Agriculture Press, pp. 89–92.
Jeffrey, A., Simmons, W.S., Currie, K.N., Eshleman, K.K., Susan, M., Tim, L.N., Bob, R.P., Carolyn, L.T., 2008. Forest to reclaimed mine land use change leads to altered ecosystem structure and function. Ecol. Appl. 18, 104–118.
Jiao, F., Wen, Z.M., An, S.S., 2011. Changes in soil properties across a chronosequence of vegetation restoration on the Loess Plateau of China. Catena 86, 110–116.
Lei, T.W., Chuo, R.Y., Zhao, J., Shi, X.N., Liu, L., 2010. An improved method for shallow water flow velocity measurement with practical electrolyte input. J. Hydrol. 390, 45–56.
Lei, T.W., Mao, L.L., Li, X., Liu, H., Huang, X.F., Zhang, Y.N., 2007. Method for measuring soil infiltrability with linear run-on of water. Trans. Chin. Soc. Agric. Eng. 23 (1), 1–5.
Lei, T.W., Yan, Y., Shi, X.N., Chuo, R.Y., Zhao, J., 2013. Measuring velocity of water flow within gravel layer with electrolyte tracer method under pulse boundary model. J. Hydrol. 500, 37–44.
Leung, A.K., Garg, A., Coo, J.L., Ng, W.W., Hau, B.C.H., 2015. Effects of the roots of *Cynodon dactylon* and *Schefflera heptaphylla* on water infiltration rate and soil hydraulic conductivity. Hydrol. Process. 29 (15), 3342–3354.
Li, J.X., He, B.H., Mei, X.M., Liang, Y.L., Xiong, J., 2013. Effects of different planting modes on the soil permeability of sloping farmlands in purple soil area. Chin. J. Appl. Ecol. 24 (3), 725–731.
Liu, X.P., He, Y.H., Zhang, T.H., Zhao, X.Y., Li, Y.Q., Zhang, L.M., Wei, S.L., Yun, J.Y., Yue, X.F., 2015. The response of infiltration depth, evaporation, and soil water replenishment to rainfall in mobile dunes in the Horqin Sandy Land, Northern China. Environ. Earth Sci. 73, 8699–8708.
Mao, L.L., Lei, T.W., Bralts, V.F., 2011. An analytical approximation method for the linear source soil infiltrability measurement and its application. J. Hydrol. 411, 169–177.
Meek, B.D., Rechel, E.A., Carter, L.M., DeTar, W.R., 1989. Changes in infiltration under alfalfa as influenced by time and wheel traffic. Soil Sci. Soc. Am. J. 53, 238–241.
Obi, M.E., 1999. The physical and chemical responses of a degraded sandy clay loam soil to cover crops in southern Nigeria. Plant Soil 211, 165–172.
Osuji, G.E., Okon, M.A., Chukwuma, M.C., 2010. Infiltration characteristics of soils under selected land use practices in Owerri, southeastern Nigeria. World J. Agric. Sci. 6 (3), 322–326.
Scanlan, C.A., Hinz, C., 2010. Insights into the processes and effects of root-induced changes to soil hydraulic properties. In: Proceedings of the 19th World Congress of Soil Science, 2: Brisbane, Australia, 41–44.
Shrestha, R.K., Lal, R., 2011. Changes in physical and chemical properties of soil after surface mining and reclamation. Geoderma 161, 168–176.
Sun, P.P., Mao, L.L., Zhao, J., Lei, T.W., 2013. Effect of flow rate on soil infiltrability measurement with the automatic system. Sci. Soil Water Conserv. 11 (2), 14–18.
Wang, G.L., Liu, G.B., Zhou, S.L., 2003. The effect of vegetation restoration on soil stable infiltration rates in small watershed of loess gully region. J. Nat. Res. 18 (5), 529–534.
Wang, X.P., Li, X.R., Xiao, H.L., Berndtsson, R., Pan, Y.X., 2007. Effects of surface characteristics on infiltration patterns in an arid shrub desert. Hydrol. Process. 21, 72–79.
Wang, X.P., Cui, Y., Pan, Y.X., Li, X.R., Yu, Z., Young, M.H., 2008. Effects of rainfall characteristics on infiltration and redistribution patterns in revegetation-stabilized desert ecosystems. J. Hydrol. 358, 134–143.
Wu, G.L., Zhang, Z.N., Wang, D., Shi, Z.H., Zhu, Y.J., 2014. Interactions of soil water content heterogeneity and species diversity patterns in semi-arid steppes on the Loess Plateau of China. J. Hydrol. 519, 1362–1367.
Yang, Z., Hao, H.M., Wang, D., Chang, X.F., Zhu, Y.J., Wu, G.L., 2015. Revegetation of artificial grassland improve soil organic and inorganic carbon and water of abandoned mine. J. Soil Sci. Plant Nutr. 15 (3), 629–638.
Zhang, Z.W., Zhu, Z.X., Wang, Y., 2010. Soil infiltration capacity and its influencing factors of different land use types in karst slope. Trans. Chin. Soc. Agric. Eng. 26 (6), 71–76.
Zhao, Y.G., Wu, P.T., Zhao, S.W., Feng, H., 2013. Variation of soil infiltrability across a 79-year chronosequence of naturally restored grassland on the Loess Plateau, China. J. Hydrol. 504, 94–103.